
MARSRETRIEVAL: BENCHMARKING VISION-LANGUAGE MODELS FOR PLANETARY-SCALE GEOSPATIAL RETRIEVAL ON MARS

Shuoyuan Wang

Department of Statistics and Data Science
Southern University of Science and Technology
Shenzhen, China
wangsy2024@mail.sustech.edu.cn

Yiran Wang

Department of Earth and Space Sciences
Southern University of Science and Technology
Shenzhen, China
wangyr@sustech.edu.cn

Hongxin Wei*

Department of Statistics and Data Science
Southern University of Science and Technology
Shenzhen, China
weihx@sustech.edu.cn

February 17, 2026

ABSTRACT

Data-driven approaches like deep learning are rapidly advancing planetary science, particularly in Mars exploration. Despite recent progress, most existing benchmarks remain confined to closed-set supervised visual tasks, failing to support text-guided retrieval for geospatial discovery in modern planetary exploration. To address this gap, we introduce MarsRetrieval, an extensive retrieval benchmark for evaluating the utility of vision-language models in Martian geospatial discovery. Specifically, MarsRetrieval organizes evaluation into 3 complementary tasks: (1) paired image–text retrieval, (2) landform retrieval and (3) global geo-localization, covering multiple spatial scales and diverse geomorphic origins. We further propose a unified retrieval-centric protocol to benchmark representative architectures for multimodal embedding, including contrastive dual-tower encoders and generative vision–language models. Comprehensive evaluation demonstrates that MarsRetrieval poses a significant challenge, with the strongest foundation models often failing to distinguish domain-specific geomorphic distinctions. In addition, we show that domain-specific fine-tuning is critical for generalizable geospatial discovery in planetary settings. By grounding evaluation in scientifically-motivated Martian challenges, MarsRetrieval aims to bridge the gap between multimodal AI capabilities and the needs of real-world planetary research. Our Code is available at <https://github.com/ml-stat-Sustech/MarsRetrieval>.

1 Introduction

Planetary science plays a pivotal role in understanding the formation, evolution, and habitability of worlds beyond Earth. Given its well-preserved record of planetary-scale processes (e.g., geological record, climate history, past aqueous activity), Mars serves as one of the most accessible and scientifically valuable targets in the Solar System [1]. As high-resolution imagery from orbiters and rovers grows to unprecedented volumes, deep learning has emerged as a significant tool in various planetary science tasks, such as terrain classification [2, 3], landform mapping [4, 5] and autonomous rover navigation [6, 7]. These advancements greatly accelerate scientific workflows and reduce human bias in interpretation.

*Corresponding author.

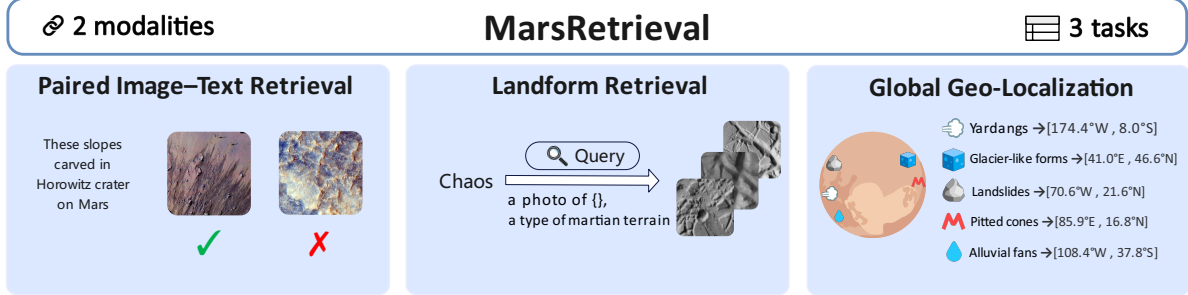


Figure 1: An overview of MarsRetrieval categories with examples. The benchmark consists of 3 challenging tasks for cross-modal retrieval in Martian exploration. See Table 1 for details about capabilities measured and other information.

The sustained progress in planetary science largely depends on high-quality benchmarks that facilitate reproducible evaluations across models. A recent representative benchmark for planetary science is Mars-Bench [8], which consolidates 20 Mars-related tasks covering image classification, semantic segmentation, and object detection. However, Mars-Bench primarily focuses on closed-set supervised visual tasks. This limitation is significant in real-world Martian research, which frequently involves language-guided discovery. In practice, researchers often start from expert textual concepts to align with corresponding Martian imagery, thereby identifying novel geological patterns and analyzing their planetary-scale spatial distributions. Consequently, Vision-Language Models (VLMs) emerge as a promising solution for bridging scientific language and imagery. Although VLMs have demonstrated remarkable success in other scientific fields (e.g., medical imaging [9, 10], chemistry [11, 12], earth observation [13, 14]), the community still lacks a standardized evaluation protocol to assess their practical utility for planetary exploration.

To address this gap, we introduce MarsRetrieval, a comprehensive retrieval benchmark for evaluating the applicability of vision-language models in Martian exploration. As shown in Figure 1, MarsRetrieval comprises 3 evaluation tasks: (1) **Paired Image-Text Retrieval** measures foundational vision-language alignment using curated Martian image-text pairs. We cover diverse spatial scales —from global orbital mosaics to rover-level microscopic imagery. (2) **Landform Retrieval** evaluates concept-to-instance generalization across 48 geomorphic categories organized by 7 major geological origins (e.g., Aeolian, Volcanic and Fluvial processes). This task supports rapid scientific hypothesis verification at the concept level. (3) **Global Geo-Localization** localizes scientific concepts within a global mosaic [15, 16] comprising over 1.4 million CTX tiles under massive background noise, facilitating planetary-scale applications such as global geomorphic cataloging. Overall, MarsRetrieval provides a holistic benchmark for evaluating VLM practical utility in representative Martian scientific tasks.

We establish strong baselines by benchmarking a broad spectrum of state-of-the-art foundation models under a unified retrieval-centric protocol. Our evaluation encompasses several distinct architectures including contrastive dual-tower VLMs (e.g., CLIP [17]), MLLM-based VLMs (e.g., Qwen3-VL-Embedding [18]) and Vision-only Foundation Models (e.g., DINOv3 [19]). Results show that MarsRetrieval is highly challenging: even strong foundation models often struggle to capture Martian geomorphic cues. We further find that domain-specific fine-tuning substantially improves generalizable geospatial discovery. Overall, MarsRetrieval serves as a standardized evaluative framework for quantifying the reliability of VLMs for future Martian exploration and scientific analysis. Furthermore, the proposed evaluation paradigm can be readily adapted to other autonomous planetary explorations, facilitating the development of foundation models for deep-space discovery.

2 Related Works

Deep Learning in Planetary Science. In recent years, the rapid progress of deep learning has substantially accelerated data analysis workflows in planetary science. Enabled by advances in model architecture and the availability of large-scale orbital and rover-level imagery, several deep learning models have achieved competitive performance on Mars-related tasks including terrain classification [2, 3, 20], feature analysis [21, 22], instance segmentation [23, 24, 25], autonomous navigation [6, 7], global geology mapping [4, 26, 27, 5], etc. Complementing these task-specific works, broader surveys argue that machine learning is becoming an essential tool for Martian geomorphology and exploration science [28]. Despite recent advances, planetary machine learning still lacks standardized datasets and evaluation protocols that have catalyzed progress in other scientific domains. Existing benchmarks, such as Mars-Bench [8], which consolidates 20 tasks spanning classification, segmentation, and object detection. Alongside such broad benchmarks, specialized datasets have emerged to tackle specific geomorphic challenges, such as landslide segmentation [29],

Table 1: An Overview of MarsRetrieval tasks. The table summarizes the data construction and capability dimensions in MarsRetrieval. We denote the modalities with I=image, T=text. “Manual Validation” denotes extra human verification.

| Task | Data Sources | Manual Validation | Abilities Assessed | Modalities |
|-----------------------------|------------------|-------------------|---|------------------------------------|
| Paired Image–Text Retrieval | Public + Curated | ✓ | fine-grained vision-language alignment | $T \rightarrow I; I \rightarrow T$ |
| Landform Retrieval | CTX, HiRISE | ✓ | concept-to-instance generalization | $T \rightarrow I$ |
| Global Geo-Localization | CTX | ✗ | planetary-scale distribution estimation | $T \rightarrow I; I \rightarrow I$ |

pitted cone segmentation [30]. However, these benchmarks primarily focus on closed-set supervised visual tasks, which are insufficient for assessing the cross-modal understanding required for modern language-driven planetary research. MarsRetrieval addresses this gap by utilizing a retrieval-centric evaluation protocol. It provides curated datasets and standardized metrics for the evaluation of various vision-language models. By doing so, MarsRetrieval provides a foundational resource for the emerging planetary ML community, facilitating reproducible research, fair model comparison, and the development of foundation model for deep-space exploration.

Vision-language Embedding Models. Vision-Language models (VLMs) have revolutionized multimodal understanding by learning joint representations from vast image-text pairs. Foundational architectures like CLIP [17] and its variants, such as SigLIP [31] and PE-Core [32], utilize dual-encoder and contrastive learning for cross-modal alignment by mapping images and text into a unified embedding space. The image and text representations can further be transferred to a wide range of downstream tasks (e.g., classification, retrieval, and generation). Beyond dual encoders, multimodal large language models (MLLMs) [33, 34, 35] couple a vision encoder with an autoregressive LLM to enable visual reasoning and instruction-following capabilities. Recently, a growing line of work adapts MLLMs into embedding models by extracting a fixed-dimensional representation from the LLM hidden states (e.g., pooling or the EOS/last-token state) and fine-tuning with retrieval-oriented contrastive learning, such as E5-V [36], GME [37], VLM2Vec-V2 [38] and Qwen3-VL-Embedding [18]. To systematically assess the utility of these diverse architectures in planetary science, we adopt a unified, retrieval-centric evaluation protocol. We conduct an extensive evaluation of both dual-encoder VLMs and the MLLM-based embedding models across the 3 core tasks of MarsRetrieval to quantify their effectiveness for Martian geospatial discovery.

3 Benchmark Overview

Existing Mars-related benchmarks, such as Mars-Bench [8], have established a standardized evaluation for planetary science. However, these benchmarks primarily focus on task-specific and closed-set supervised vision tasks with single-modality inputs. This leaves a significant gap in evaluating the multimodal understanding of modern VLMs, which are essential for language-driven planetary research. To bridge this gap, we introduce MarsRetrieval, a comprehensive retrieval-centric geospatial benchmark to evaluate diverse VLM embedding models on 3 Mars-related tasks.

Evaluation Protocol. MarsRetrieval adopts a retrieval-based evaluation protocol, which evaluates whether matched items are ranked above mismatched candidates in a joint representation space. Formally, given a query q and a gallery of candidates $G = \{c_1, c_2, \dots, c_n\}$, the model should rank the candidates based on their similarity $s(f(q), f(c_i))$, where $f(\cdot)$ represents the model’s embedding function and $s(\cdot, \cdot)$ is typically the cosine similarity. By utilizing this protocol, MarsRetrieval can objectively measure zero-shot understanding of VLMs across diverse tasks without the need for task-specific fine-tuning.

Design Principles. Under the unified retrieval-centric protocol mentioned above, MarsRetrieval proposes three complementary tasks that form a comprehensive evaluation: from foundational perception to planetary-scale application. As summarized in Table 1, these tasks are designed to evaluate distinct capability dimensions: (1) Paired Image–Text Retrieval assesses foundational feature alignment by matching fine-grained scientific descriptions with corresponding Martian imagery across diverse orders of spatial scale. (2) Landform Retrieval evaluates concept-to-instance generalization by retrieving diverse instances from 48 long-tailed geomorphic categories spanning multiple geological origins (e.g., aeolian, volcanic) using their scientific concepts. (3) Global Geo-Localization simulates planetary-scale discovery by localizing target landforms within a global archive of 1.4 million tiles under massive background noise. We describe three tasks and their datasets and evaluation protocols in Sections 4, 5, and 6, respectively.

4 Task 1: Paired Image–Text Retrieval

We formulate task 1 as a one-to-one cross-modal retrieval task, where a model should align highly specialized planetary-science descriptions with the corresponding Martian image (and vice-versa). The curated dataset consists of 2,287 Martian paired samples, spanning diverse orders of magnitude in spatial scale. As shown in Figure 2, the dataset coverage ranges from planetary-scale orbital mosaics to rover-level microscopic imagery, encompassing diverse imaging modalities, geomorphic structures, atmospheric phenomena, and instrument-related visual cues.

4.1 Dataset Construction

We construct the dataset via a multi-stage pipeline that prioritizes Mars relevance, pair quality, and broad coverage in both semantic and visual spaces.

Data Collection. We first construct a candidate pool of Martian image-text pairs from two web-scale corpora: DataComp-1B [39] and Relation-2B [40]. To ensure domain relevance, we employ text-based retrieval over captions using FAISS [41] with Qwen3-Embedding-0.6B [42]. We cover major Mars-related concepts in the query set, including diverse core geomorphic processes and landforms, atmospheric phenomena, and heterogeneous remote-sensing data across multiple scales (e.g., CTX [15, 16], HiRISE [43, 44]).

Data Filtering. To ensure pair correctness and domain specificity of Mars, we apply complementary automatic signals to filter out noise pairs. A candidate pair is retained only if it satisfies thresholds across all three metrics:

- **CLIP score:** We use CLIPScore [45] with ViT-H-14-378-quickgelu to quantify basic cross-modal similarity.
- **LLM relevance confidence:** we verify whether the caption refers to Mars-related concepts using token-level confidence [46] with Qwen2.5-7B [47].
- **MLLM consistency confidence:** We use Qwen2.5-VL-7B-Instruct [34] to assess whether the visual evidence is grounded in the text and jointly relevant to Mars.

We provide the detailed strategy for data filtering in Appendix A.1. The prompts used for LLM and MLLM confidence are shown in Figure 8 and Figure 9, respectively.

Diversity Sampling. To improve coverage of scientific concepts and visual appearances, we select a compact yet diverse subset via a two-stage K-center Greedy strategy. First, we select a subset that maximizes semantic diversity in the text embedding space using Qwen3-Embedding-0.6B [42]. Second, within the subset, we further maximize coverage in the visual feature space using DINOv3 [19].

Caption Refinement. For the final refined subset, we utilized Qwen3-VL-235B-A22B-Instruct [48] to perform caption rewriting. We rewrite more fine-grained captions while remaining strictly grounded in visible evidence.

Expert Validation. To guarantee scientific authority, planetary scientists validate the rewritten captions with the corresponding images to ensure Mars relevance and correctness.

4.2 Evaluation set-up and metrics

Evaluation Setup. We evaluate the model on bidirectional image–text retrieval. All image-text pairs are encoded into a shared embedding space and the embeddings are L2-normalized. Given a query in one modality (e.g., Image), candidates in the other modality (e.g., Text) are ranked by cosine similarity. The rank of the paired ground-truth instance is recorded to calculate retrieval metrics.

Metrics. We evaluate performance using standard retrieval metrics **Recall@1 (R@1)** and **Recall@10 (R@10)**, which measure the hit rate of the ground-truth match within the top- K ranked candidates. In addition, to better characterize ranking quality beyond a fixed cutoff, we report **Mean Reciprocal Rank (MRR)**, which rewards placing the true match

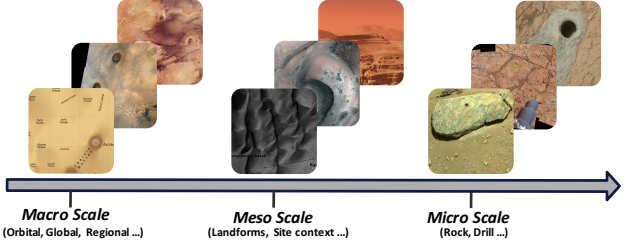


Figure 2: Planetary scale coverage in task 1 (Paired Image–Text Retrieval). We include Martian paired samples from orbital terrain to rover instrumentation.

as high as possible. Finally, to measure overall stability and provide a robust summary that is less sensitive to outliers, we report **Median Rank (MedR)**, where lower is better. Formal definitions are shown in Appendix B.1.

5 Task 2: Landform Retrieval

We formulate Task 2 as a text-to-image retrieval task. Given a textual prompt of a geomorphic concept, the model should retrieve its multiple corresponding visual instances from a Martian gallery. The dataset comprises 1,185 carefully curated image patches and follows a two-level geomorphology taxonomy. As shown in Figure 3, we organize the dataset into 7 major genetic classes. The sub-classes are the actual retrieval units, which consist of 48 landforms and follow a long-tailed distribution (See Figure 12 in Appendix). A key challenge is that Martian landforms do not conform to a single canonical appearance. Specifically, Task 2 emphasizes 2 challenges: (1) Morphological diversity (e.g., different erosion stages, slopes, scales), (2) Spatial diversity (e.g., varying latitudes and illumination).

5.1 Dataset Construction

Task 2 primarily probes whether a model can remain robust across variations in morphology and geography. To this end, we employed a hybrid pipeline combining foundation model discovery with curation from CTX and HiRISE imagery.

Data Collection. We follow the MarScope framework [4] and perform large-scale text-to-image similarity search across a global Mars mosaic at default scale. To mitigate the model bias, we employ MarScope with different training weight configurations. For each landform subclass, we retrieve the top-100 candidates based on cosine similarity. Moreover, to cover rare classes that are difficult to observe reliably at the default observation scale of MarScope (e.g., Boulder Track, Fractured Mounds, etc.), we supplement the dataset with targeted high-resolution image patches curated from public-domain CTX [49] and HiRISE [43, 44] data. To ensure the fairness of our evaluation, we further provide a detailed analysis of model generalization on these curated classes without using MarScope in Appendix C.2 (See Figure 8).

Expert Validation. Planetary geomorphology experts then manually verify the collected candidates to ensure each retained instance exhibits clear, discriminative characteristics consistent with its target landform concept. Crucially, we preserve intra-class diversity by retaining samples from different latitudes and morphologies.

5.2 Evaluation set-up and metrics

Evaluation Setup. We evaluate text-to-image retrieval under a multi-positive setting. For each sub-class, we generate a prototype query embedding averaged from prompt templates using the model’s text encoder. We provide the detailed information in Appendix A.2 and the ablation in Figure 5. The visual database is pre-indexed offline using the model’s image encoder. During retrieval, all database images are ranked by cosine similarity, and the ground-truth positives are all images annotated with the corresponding subclass.

Metrics. We report metrics for multi-positive retrieval under long-tail class frequencies. Our primary metric is **macro-mAP**, which computes Average Precision per sub-class and then averages across concepts. We also report Normalized Discounted Cumulative Gain **nDCG@10** to assess whether representative positives are prioritized early in the ranked list. Finally, we report **Hits@10** to measure whether at least one true instance appears in the top-10 results. Formal implementation details are provided in the Appendix B.2.

6 Task 3: Global Geo-Localization

We formulate Task 3 as a planetary-scale geo-localization problem. Given a query (text or image), the model is expected to retrieve all relevant geographic locations from the global CTX mosaic [15, 16]. The set of predicted coordinates

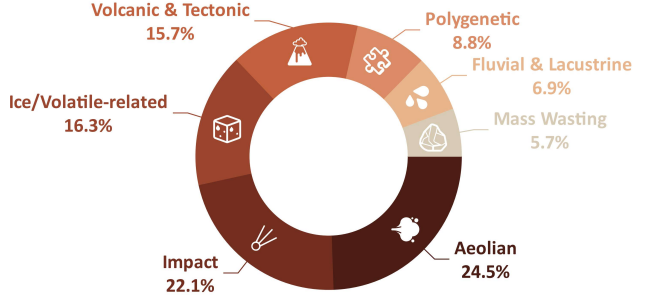


Figure 3: Dataset distribution across the 7 major genetic classes of Martian landforms in task 2 (Landform Retrieval). The detailed distribution of subclasses is shown in Figure 12.

could further form a coherent global distribution map on the Mars surface rather than a small set of top-ranked examples. Unlike Tasks 1&2, which operate on a closed candidate gallery, Task 3 emphasizes real-world deployment under extreme class imbalance: sparse positives embedded in massive background noise. We present the global distributions of the five landforms in Figure 4, utilizing reference points compiled from published scientific catalogs.

6.1 Dataset Construction

Global Mosaic Tiling. Following MarScope [4], we construct a planetary-scale retrieval index by partitioning the global Mars CTX mosaic (6 m/pixel) [49] into a large number of overlapping tiles. Specifically, we adopt a default angular resolution of 0.2° (approximately 12 km at the equator) to generate a global gallery comprising over 1.4 million patches. Each patch is indexed with precise planetocentric coordinates via spherical projection.

Ground Truth Curation. To enable quantitative evaluation, we aggregate ground-truth locations from published global catalogs of Martian landforms, including Alluvial fans [50], Glacier-like forms [51], Landslides [52], Pitted cones [53], and Yardangs [54]. For each landform type, the published catalogues provide a set of reference points, which is expressed as planetocentric latitude and longitude (See detailed distribution in Figure 4).

6.2 Evaluation set-up and metrics

Evaluation Setup. We evaluate two query modes: text-based and image-based. The prompt template and image queries are shown in Appendix A.2 and Appendix A.3, respectively. The image embeddings are extracted using the model’s visual encoder and stored by FAISS in advance. For each target landform, we retrieve the top- K (e.g., $K = 20,000$) candidates from the global index by cosine similarity and map them back to form a predicted point set.

For quantitative validation, we evaluate retrieval outputs against published global landform catalogues as point sets. We formulate evaluation as a proximity-based point-set matching problem between the prediction set and the catalogue reference set. Since exact coordinate coincidence is infeasible due to continuous geography, we consider an image patch to be a true positive if the predicted coordinate falls within a physical spatial tolerance radius r (e.g., $r = 0.5^\circ$) of a ground-truth entry. We conduct the approximate calculation via KDTree [55].

Metrics. Given the extreme sparsity of positive samples against the global background, standard accuracy metrics are unsuitable. We report **AUPRC** (Area Under Precision-Recall Curve) as the primary metric, which rigorously assesses the trade-off between retrieval precision and recall without being biased by the massive volume of true negatives. Additionally, we report the optimal F1 score **F1@ K^*** on the PR curve to quantify the best possible alignment between the predicted global map and the human-curated catalogue. Formal definitions are provided in the Appendix B.3.

7 Experiments

7.1 Experimental Setup

Models. To establish a comprehensive benchmark, we evaluate a broad range of foundation models on MarsRetrieval. We categorize the models into 3 groups. (1) **Dual-encoder vision-language models**: CLIP-DFN2B [56], BGE-VL-large [57], AIMV2-224 [58], SigLIP [59], SigLIP2 [31] and PE-Core [32]. (2) **MLLM-based embedding models**: E5-V [36], GME [37], B3++ [60], jina-embeddings-v4 [61], VLM2Vec-V2 [38], Ops-MM-embedding-v1 [62] and Qwen3-VL-Embedding [18]. (3) We also incorporate **Vision-only Foundation Models** like DINOv3 [19] and AIMV2-448 [58] for the image retrieval in Task 3 (Global Geo-Localization). Moreover, we include **MarScope** [4], a planetary science-specialized model fine-tuned from CLIP-DFN2B. We also verified the training set of MarScope does not overlap with MarsRetrieval. For fair comparison, the encoder-based models are selected at the ViT-L/14 or equivalent scale (0.4B), while most MLLM-based embedding models operate at the 2B parameter scale.

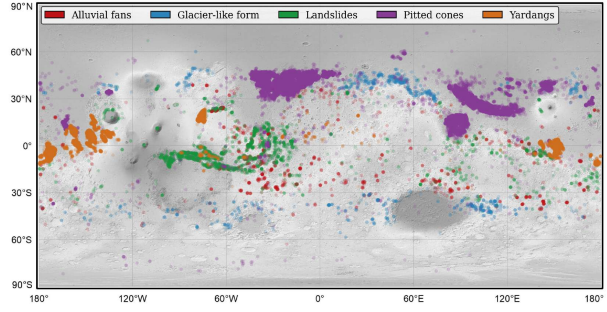


Figure 4: Global ground-truth distribution from scientific catalogs [50, 51, 52, 53, 54] for Task 3 (Global Geo-Localization).

Table 2: Retrieval results of Task 1 (Paired Image-Text Retrieval) using refined captions. We report bidirectional retrieval performance on various vision-language models. Best results are in bold and second best are underlined.

| Model | Backbone | Size | T→I | | | | I→T | | | |
|-----------------------------|------------|------|--------------|--------------|--------------|-----------|--------------|--------------|--------------|-----------|
| | | | R@1 | R@10 | MRR | MedR | R@1 | R@10 | MRR | MedR |
| <i>Encoder-based Models</i> | | | | | | | | | | |
| DFN2B-CLIP-ViT-L-14 | ViT-L/14 | 0.4B | 13.12 | 32.36 | 19.83 | 47 | 9.88 | 27.15 | 15.87 | 68 |
| ViT-L-16-SigLIP-384 | ViT-L/16 | 0.4B | 15.65 | 33.84 | 21.91 | 48 | 14.82 | 30.96 | 20.57 | 58 |
| BGE-VL-large | ViT-L/14 | 0.4B | 2.93 | 12.55 | 6.37 | 188 | 9.18 | 27.11 | 15.19 | 65 |
| aimv2-large-patch14-224 | ViT-L/14 | 0.4B | 7.87 | 22.39 | 13.00 | 97 | 5.33 | 17.67 | 9.77 | 142 |
| ViT-L-16-SigLIP2-512 | ViT-L/16 | 0.4B | <u>21.47</u> | 42.37 | <u>28.59</u> | 21 | 17.45 | 37.12 | 24.20 | <u>32</u> |
| PE-Core-L-14-336 | ViT-L/14 | 0.4B | 21.64 | 45.78 | 29.94 | 14 | 20.24 | <u>43.86</u> | 28.35 | 16 |
| MarScope | ViT-L/14 | 0.4B | 18.01 | <u>45.04</u> | 26.87 | <u>15</u> | <u>17.49</u> | 44.43 | <u>26.56</u> | 16 |
| <i>MLLM-based Models</i> | | | | | | | | | | |
| E5-V | LLaVA-Next | 8B | 11.37 | 21.43 | 15.03 | 168 | 12.24 | 23.66 | 16.28 | 138 |
| gme | Qwen2-VL | 2B | 14.34 | 27.81 | 19.20 | 102 | 14.17 | 27.72 | 18.97 | 87 |
| B3++ | Qwen2-VL | 2B | 8.09 | 19.15 | 12.01 | 203 | 7.08 | 15.83 | 10.34 | 237 |
| jina-embeddings-v4 | Qwen2.5-VL | 3B | 14.52 | 27.11 | 18.98 | 115 | 12.59 | 25.05 | 17.12 | 139 |
| VLM2Vec-V2.0 | Qwen2-VL | 2B | 6.47 | 18.01 | 10.82 | 158 | 9.62 | 22.13 | 13.92 | 135 |
| Ops-MM-embedding-v1 | Qwen2-VL | 2B | 18.23 | 32.14 | 23.21 | 66 | 16.92 | 31.61 | 22.28 | 61 |
| Qwen3-VL-Embedding | Qwen3-VL | 2B | 16.97 | 33.45 | 22.55 | 62 | 15.96 | 33.71 | 22.24 | 47 |

Implementation Details. Across all three tasks, we adopt a unified embedding-based retrieval protocol. Images and texts are encoded independently using the corresponding encoders of each model. Embedding models are evaluated using their official public checkpoints with default preprocessing and recommended input resolutions. All embeddings are pre-computed offline and L2-normalized. During inference time, only the query embedding (text or image) is encoded and compared against the pre-indexed gallery using cosine similarity.

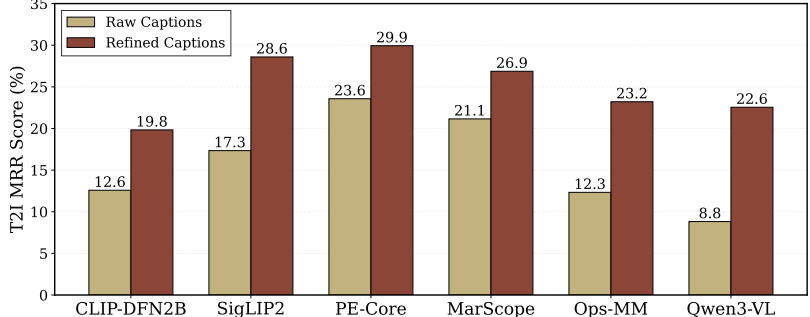


Figure 5: Ablation on caption refinement in Paired Image–Text Retrieval (task 1). The results on MRR indicate high-quality captioning leads to stronger vision–language alignment.

7.2 Paired Image–Text Retrieval

Encoder-based models demonstrate superior performance in vision–language alignment. As shown in Table 2, encoder-based models (e.g., PE-Core-L-14) achieve better recall and lower median rank than MLLM-based models across both retrieval directions. Furthermore, domain-specific post-training can significantly boost retrieval capabilities. MarScope improves substantially over its pre-trained version (CLIP-DFN2B), which gain +12.68% on R@10 (T→I) and +17.28% (I→T). Notably, PE-Core-L-14-336 shows the best overall retrieval performance without any task-specific finetuning. Nevertheless, the absolute performance still remains moderate, indicating challenges in precisely ranking fine-grained, multiscale Martian image-text pairs.

Caption refinement consistently improves retrieval quality. As illustrated in Figure 5, all evaluated models yield consistent MRR gains when applying the refined captions (See Section 4.1). The benefit shows that the refined captions can successfully eliminate image-text irrelevant noise and provide more precise and discriminative descriptions of Martian features. Notably, MLLM-based models benefit the most from this refinement, where Qwen3-VL and Ops-MM improve MRR by 13.8% and 10.9%, respectively. We present the results with raw caption in Appendix C.1 (See Figure 7). Overall, the results demonstrate that the quality of captions is crucial for vision–language alignment in planetary science tasks.

Table 3: Ablation on model scale in Paired Image-Text Retrieval (task 1). Best results within each family are in bold.

| Family | Model | $T \rightarrow I$ (%) | $I \rightarrow T$ (%) |
|-----------------------------|---------|-----------------------|-----------------------|
| <i>Encoder-based Models</i> | | | |
| PE-core | B16-224 | 26.47 | 20.28 |
| | L14-336 | 29.94 | 28.35 |
| | G14-448 | 33.64 | 32.44 |
| <i>MLLM-based Models</i> | | | |
| Qwen3-VL | 2B | 22.55 | 22.24 |
| | 8B | 23.20 | 24.12 |

Table 4: Retrieval results of Landform Retrieval (task 2). Best results are in bold and second-best results are underlined.

| Model | mAP | nDCG@10 | Hits@10 |
|-----------------------------|--------------|--------------|--------------|
| <i>Encoder-based Models</i> | | | |
| DFN2B-CLIP-ViT-L-14 | 9.48 | 12.39 | 47.92 |
| ViT-L-16-SigLIP-384 | 8.59 | 9.46 | 37.50 |
| BGE-VL-large | 7.16 | 6.89 | 31.25 |
| aimv2-large-patch14-224 | 6.12 | 7.07 | 43.75 |
| ViT-L-16-SigLIP2-512 | 9.59 | 10.84 | 60.42 |
| PE-Core-L-14-336 | <u>20.93</u> | <u>25.80</u> | <u>72.92</u> |
| MarScope | 71.89 | 74.42 | 93.75 |
| <i>MLLM-based Models</i> | | | |
| E5-V | 6.20 | 5.04 | 27.08 |
| gme | 6.80 | 6.44 | 45.83 |
| B3++ | 5.26 | 4.58 | 27.08 |
| jina-embeddings-v4 | 6.57 | 4.67 | 31.25 |
| VLM2Vec-V2.0 | 5.60 | 3.86 | 22.92 |
| Ops-MM-embedding-v1 | 9.30 | 9.62 | 41.67 |
| Qwen3-VL-Embedding | 8.68 | 9.92 | 39.58 |

Scaling model parameters yields better retrieval performance. As shown in Table 3, larger backbones yield steady improvements in bidirectional MRR. Specifically, the SigLIP2 family shows a steady increase in I→T evaluation from 20.28 (base-16-224) to 32.44 (G14-448). This consistent scaling trend demonstrates that increased model size can better capture the complex visual information required for authentic Martian discovery and scientific analysis.

7.3 Landform Retrieval

Domain-specific fine-tuning is essential for Martian landform retrieval. Table 4 shows that Task 2 is substantially more challenging and domain-sensitive than generic image-text retrieval. Among all models, MarScope achieves a dominant performance over all general pre-trained foundation models with 71.89% for mAP and 93.75% for Hits@10. In contrast, even the strongest baseline (PE-Core-L-14-336) only reaches an mAP of 20.93%, which is nearly 50% lower than that of MarScope. This substantial gap highlights that general vision-language models lack the expertise of planetary science to distinguish subtle Martian geomorphic features.

Prompt ensemble provides consistent performance gains. To verify the effectiveness of the prompt ensemble mentioned in Section 5.2, we provide an ablation study in Table 5. For MarScope, ensembling 7 templates yields the highest macro-mAP of 72.44%, a gain of +3.70% over the single-prompt baseline. Moreover, the incremental gains for other general models tend to saturate at 3 templates. To maintain an optimal balance between retrieval accuracy and simplicity, we adopt an ensemble of three prompts as the default setting throughout our main evaluation.

7.4 Global Geo-Localization

Text-based retrieval can generalize to diverse Martian landforms after domain-specific fine-tuning. We provide the results for Task 3 (Global Geo-Localization) in Table 6. The results show that MarScope consistently achieves the strongest text-based retrieval performance across all 5 landform categories. For example, MarScope attains high AUPRC on Alluvial Fans (14.88), Landslides (25.62), Pitted Cones (71.31), and Yardangs (65.38), indicating robust alignment between geomorphology terminology and landform image patches. In contrast, general encoder-based VLMs and MLLM-based models reach only moderate or low AUPRC values, which is consistent with the observation shown in Task 2. These results indicate that while MLLMs possess broad internal knowledge, they fail to establish the precise

Table 5: Ablation on different prompt templates in Landform Retrieval (task 2). We use 3 templates throughout the paper.

| Model | 1 | 3 | 5 | 7 | 10 |
|---------------------|-------|--------------|-------|--------------|-------|
| MarScope | 68.74 | 71.89 | 71.87 | 72.44 | 72.32 |
| PE-Core-L-14-336 | 20.67 | 20.93 | 20.06 | 19.68 | 19.84 |
| Qwen3-VL-Embedding | 8.43 | 8.69 | 7.63 | 7.73 | 7.51 |
| Ops-MM-embedding-v1 | 9.52 | 9.62 | 7.28 | 8.35 | 8.50 |

Table 6: Retrieval results of Global Geo-Localization (Task 3) on various foundation models. We report AUPRC for both text-based and image-based retrieval across five Martian landforms. Best results are in bold and second-best results are underlined.

| Model | Alluvial Fans | | Glacier-Like Forms | | Landslides | | Pitted Cones | | Yardangs | |
|---------------------------|---------------|--------------|--------------------|--------------|--------------|--------------|--------------|--------------|--------------|--------------|
| | Text | Image | Text | Image | Text | Image | Text | Image | Text | Image |
| <i>Encoder-based VLMs</i> | | | | | | | | | | |
| DFN2B-CLIP-ViT-L-14 | 1.47 | 2.32 | 1.96 | 17.90 | <u>29.27</u> | 4.76 | 7.29 | 16.71 | 0.24 | 28.86 |
| ViT-L-16-SigLIP-384 | <u>6.82</u> | 1.73 | 2.29 | 11.70 | 23.54 | 1.98 | 5.25 | 14.06 | 1.65 | 35.34 |
| BGE-VL-large | 1.68 | 2.74 | 1.98 | 10.39 | 29.22 | 7.10 | 1.85 | <u>26.32</u> | 1.29 | 14.59 |
| aimv2-large-patch14-224 | 1.54 | 1.11 | 2.27 | 11.65 | 26.68 | 2.04 | 1.70 | 12.26 | 1.26 | 21.86 |
| ViT-L-16-SigLIP2-512 | 1.55 | 2.94 | 6.33 | 21.97 | 25.83 | 2.48 | 3.68 | 14.87 | 1.51 | 27.79 |
| PE-Core-L-14-336 | 3.82 | 2.23 | <u>6.66</u> | 14.24 | 31.14 | 6.79 | <u>16.86</u> | 19.91 | 2.63 | 34.20 |
| MarScope | 14.88 | 12.10 | 33.65 | 36.88 | 25.62 | 13.91 | 71.31 | 40.63 | 65.38 | 56.02 |
| <i>Vision-only Models</i> | | | | | | | | | | |
| aimv2-large-patch14-448 | – | 2.38 | – | 18.03 | – | <u>8.30</u> | – | 14.23 | – | 19.47 |
| dinov3-vitl16 | – | <u>4.23</u> | – | <u>25.39</u> | – | 3.75 | – | 15.09 | – | <u>44.50</u> |
| <i>MLLM-based Models</i> | | | | | | | | | | |
| E5-V | 4.15 | 3.12 | 1.72 | 9.75 | 25.04 | 3.35 | 0.56 | 19.07 | 1.44 | 21.59 |
| gme | 1.11 | 1.42 | 1.88 | 14.66 | 4.33 | 3.13 | 0.23 | 9.45 | 0.26 | 29.16 |
| B3++ | 0.03 | 1.31 | 0.26 | 8.55 | 0.03 | 3.67 | 0.03 | 14.33 | 0.00 | 37.12 |
| jina-embeddings-v4 | 2.54 | 0.25 | 1.59 | 5.91 | 2.29 | 1.36 | 0.51 | 21.30 | 0.94 | 14.55 |
| VLM2Vec-V2.0 | 1.32 | 1.69 | 0.32 | 3.17 | 2.02 | 6.29 | 1.69 | 8.62 | 0.20 | 38.14 |
| Ops-MM-embedding-v1 | 3.67 | 1.27 | 2.65 | 11.52 | 10.39 | 2.58 | 3.47 | 18.37 | 0.66 | 36.33 |
| Qwen3-VL-Embedding | 1.37 | 0.55 | 0.75 | 12.88 | 6.84 | 2.29 | 0.09 | 5.74 | <u>9.14</u> | 39.39 |

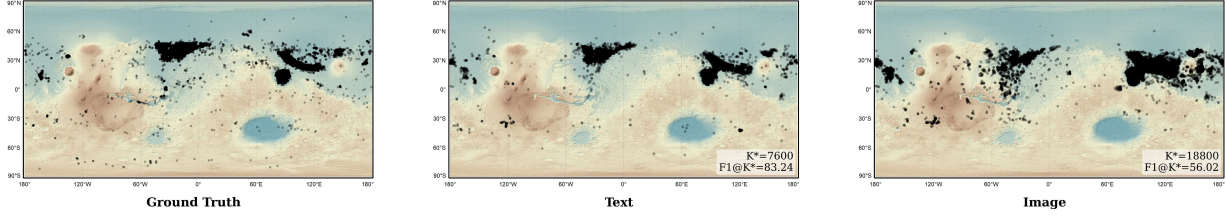


Figure 6: Global distribution of Pitted Cones in Task 3. The distribution retrieved by text-based query shows a more similar result to the ground truth, highlighting its potential for language-driven planetary discovery.

alignment between the subtle semantic and morphological characteristics of Martian landforms. We provide more results on the optimal F1 score $F1@K^*$ in Appendix C.3 (See Table 9 and Figure 13). Overall, the results highlight that generic multimodal representations are insufficient for expert-level Martian landform retrieval without explicit fine-tuning using planetary knowledge.

Text-based query shows better generalization capacity than image-based query. To provide a comprehensive evaluation, we also use several image instances to conduct the image-to-image retrieval. The images are collected by planetary scientists, and we provided detailed information in Appendix A.3. The results are also presented in Table 6. In image-based retrieval, MarScope often performs better when querying with text than with images (e.g., 71.31% vs. 40.63% on Pitted Cones, 65.38% vs. 56.02% on Yardangs). To have a better view, we further visualize the predicted global distributions of Pitted Cones at the optimal retrieval point K^* in Figure 6. The distribution retrieved via text queries produces a distribution that is substantially closer to the ground-truth catalog than the image-based retrieval. We attribute this result to the inherent visual diversity of Martian landforms. Due to extreme intra-class variation in morphology, it is difficult to identify a small set of representative visual exemplars that fully characterize the diversity of each landform category. The detailed results of distribution visualization are shown in Figure 14 in the Appendix C.

Nevertheless, **image-based retrieval still remains viable for general-purpose vision models**. Several general VLMs achieve competitive AUPRC and even outperform text retrieval in specific classes (e.g., Pitted Cones and Yardangs). Notably, the vision-only model DINOv3-vitl16 reaches the strongest overall image-based AUPRC, including 17.78% on Glacier-Like Forms and 44.50% on Yardangs. These results indicate that general models can already possess reasonable visual feature representations for Martian visual discrimination, but suffer from poor planetary vision-language alignment. The observation further suggests that improving the alignment between planetary vision-language pairs is key to advancing geomorphology retrieval on Mars.

The spatial tolerance radius is essential for reasonable geo-localization evaluation. Following the evaluation protocol mentioned in Section 6.2, we conduct an ablation study on the spatial tolerance radius r to verify its necessity. We present the $F1@K^*$ scores for Landslides and Yardangs across a range of r values in Figure 7. When r is set to an extremely small value (e.g., $r = 0.01^\circ$), the $F1$ scores remain near zero (e.g., 0.13% for Landslides), making it difficult to distinguish model performance or establish scientific significance. As r increases, the metric becomes substantially more informative and stable. Hence, to balance the trade-off between localization performance and benchmark fairness, we adopt $r = 0.5^\circ$ as the default setting in this paper.

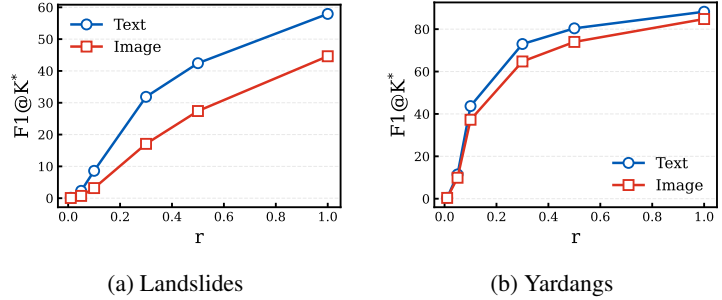


Figure 7: Ablation on the spatial tolerance radius r in Global Geo-Localization (task 3). We use $r=0.5$ throughout the paper.

8 Conclusion

In this work, we introduce MarsRetrieval, the first comprehensive retrieval-centric benchmark specifically designed to evaluate vision-language models (VLMs) for planetary-scale geospatial discovery on Mars. By organizing evaluation around three complementary and scientifically motivated tasks including Paired Image–Text Retrieval, Landform Retrieval, and Global Geo-Localization, MarsRetrieval bridges a critical gap between modern multimodal foundation models and the realistic language-driven workflows in contemporary planetary science. Comprehensive benchmarking across various foundation models reveals that MarsRetrieval remains highly challenging. Moreover, domain-specific post-training is crucial for robust and generalizable performance. Ultimately, we hope MarsRetrieval can serve as a standardized and challenging testbed to facilitate the development of next-generation foundation models for Mars and broader deep-space exploration.

References

- [1] BL Ehlmann, FS Anderson, J Andrews-Hanna, DC Catling, PR Christensen, BA Cohen, CD Dressing, CS Edwards, LT Elkins-Tanton, KA Farley, et al. The sustainability of habitability on terrestrial planets: Insights, questions, and needed measurements from mars for understanding the evolution of earth-like worlds. *Journal of Geophysical Research: Planets*, 121(10):1927–1961, 2016.
- [2] Brandon Rothrock, Ryan Kennedy, Chris Cunningham, Jeremie Papon, Matthew Heverly, and Masahiro Ono. Spoc: Deep learning-based terrain classification for mars rover missions. *AIAA space 2016*, page 5539, 2016.
- [3] Raj Gaurang Tiwari, Dibyajish Bordoloi, and Ambuj Kumar Agarwal. Marsdeepnet: A hybrid deep learning approach for mars terrain classification using modified googlenet architecture. In *2024 13th International Conference on System Modeling & Advancement in Research Trends (SMART)*, pages 638–642. IEEE, 2024.
- [4] Yiran Wang, Shuoyuan Wang, Zhaoran Wei, Jiannan Zhao, Zhonghua Yao, Zejian Xie, Songxin Zhang, Jun Huang, Bingyi Jing, and Hongxin Wei. Natural language-driven global mapping of martian landforms. *arXiv preprint arXiv:2601.15949*, 2026.
- [5] Kyle A Pearson, Eldar Noe, Daniel Zhao, Alphan Altinok, and Alexander M Morgan. Mapping “brain terrain” regions on mars using deep learning. *The Planetary Science Journal*, 5(7):167, 2024.
- [6] Shreyansh Daftry, Neil Abcouwer, Tyler Del Sesto, Siddarth Venkatraman, Jialin Song, Lucas Igel, Amos Byon, Ugo Rosolia, Yisong Yue, and Masahiro Ono. Mlnav: Learning to safely navigate on martian terrains. *IEEE Robotics and Automation Letters*, 7(2):5461–5468, 2022.

[7] Andreas Bechtold, Gerhard Paar, Filippo Garolla, Rebecca Nowak, Laura Fritz, Christoph Traxler, Oliver Sidla, and Christian Koeberl. Planetary scientific target detection via deep learning: A case study for finding shatter cones in mars rover images. *Meteoritics & Planetary Science*, 58(9):1274–1286, 2023.

[8] Mirali Purohit, Bimal Gajera, Vatsal Malaviya, Irish Mehta, Kunal Sunil Kasodekar, Jacob Adler, Steven Lu, Umaa Rebbapragada, and Hannah Kerner. Mars-bench: A benchmark for evaluating foundation models for mars science tasks. In *The Thirty-ninth Annual Conference on Neural Information Processing Systems Datasets and Benchmarks Track*, 2025.

[9] Jiazhen Pan, Che Liu, Junde Wu, Fenglin Liu, Jiayuan Zhu, Hongwei Bran Li, Chen Chen, Cheng Ouyang, and Daniel Rueckert. Medvlm-r1: Incentivizing medical reasoning capability of vision-language models (vlms) via reinforcement learning. In *International Conference on Medical Image Computing and Computer-Assisted Intervention*, pages 337–347. Springer, 2025.

[10] Sheng Zhang, Yanbo Xu, Naoto Usuyama, Hanwen Xu, Jaspreet Bagga, Robert Tinn, Sam Preston, Rajesh Rao, Mu Wei, Naveen Valluri, et al. A multimodal biomedical foundation model trained from fifteen million image–text pairs. *NEJM AI*, 2(1):A10a2400640, 2025.

[11] Jingchao Wang, Yifan He, Haote Yang, Jiang Wu, Lingli Ge, Xingjian Wei, Yinfan Wang, Linye Li, Huijie Ao, Chengjin Liu, et al. Gtr-cot: Graph traversal as visual chain of thought for molecular structure recognition. *arXiv preprint arXiv:2506.07553*, 2025.

[12] Junxian Li, Di Zhang, Xunzhi Wang, Zeying Hao, Jingdi Lei, Qian Tan, Cai Zhou, Wei Liu, Yaotian Yang, Xinrui Xiong, et al. Chemvlm: Exploring the power of multimodal large language models in chemistry area. In *Proceedings of the AAAI Conference on Artificial Intelligence*, volume 39, pages 415–423, 2025.

[13] Fengxiang Wang, Mingshuo Chen, Yueying Li, Di Wang, Haotian Wang, Zonghao Guo, Zefan Wang, Shan Boqi, Long Lan, Yulin Wang, Hongzhen Wang, Wenjing Yang, Bo Du, and Jing Zhang. GeoLLaVA-8k: Scaling remote-sensing multimodal large language models to 8k resolution. In *The Thirty-ninth Annual Conference on Neural Information Processing Systems*, 2025.

[14] Kartik Kuckreja, Muhammad Sohail Danish, Muzammal Naseer, Abhijit Das, Salman Khan, and Fahad Shahbaz Khan. Geochat: Grounded large vision-language model for remote sensing. In *Proceedings of the IEEE/CVF Conference on Computer Vision and Pattern Recognition*, pages 27831–27840, 2024.

[15] JL Dickson, BL Ehlmann, LH Kerber, and CI Fassett. Release of the global ctx mosaic of mars: an experiment in information-preserving image data processing. In *54th Lunar and planetary science conference*, volume 2806, page 2353, 2023.

[16] Michael C Malin, James F Bell III, Bruce A Cantor, Michael A Caplinger, Wendy M Calvin, R Todd Clancy, Kenneth S Edgett, Lawrence Edwards, Robert M Haberle, Philip B James, et al. Context camera investigation on board the mars reconnaissance orbiter. *Journal of Geophysical Research: Planets*, 112(E5), 2007.

[17] Alec Radford, Jong Wook Kim, Chris Hallacy, Aditya Ramesh, Gabriel Goh, Sandhini Agarwal, Girish Sastry, Amanda Askell, Pamela Mishkin, Jack Clark, et al. Learning transferable visual models from natural language supervision. In *International conference on machine learning*, pages 8748–8763. PMLR, 2021.

[18] Mingxin Li, Yanzhao Zhang, Dingkun Long, Keqin Chen, Sibo Song, Shuai Bai, Zhibo Yang, Pengjun Xie, An Yang, Dayiheng Liu, et al. Qwen3-vl-embedding and qwen3-vl-reranker: A unified framework for state-of-the-art multimodal retrieval and ranking. *arXiv preprint arXiv:2601.04720*, 2026.

[19] Oriane Siméoni, Huy V Vo, Maximilian Seitzer, Federico Baldassarre, Maxime Oquab, Cijo Jose, Vasil Khalidov, Marc Szafraniec, Seungeun Yi, Michaël Ramamonjisoa, et al. Dinov3. *arXiv preprint arXiv:2508.10104*, 2025.

[20] Sebastian Mengwall and Scott D Guzewich. Cloud identification in mars daily global maps with deep learning. *Icarus*, 389:115252, 2023.

[21] Jiannan Zhao, Yixuan Wang, Yiran Wang, Ting Huang, Shiqi Zhang, Yuan Zhao, Jun Huang, Honglei Lin, and Long Xiao. Geological diversity of paleolakes in the northwest arabia terra, mars: Implications for landing site selection of tianwen-3 mission. *Journal of Geophysical Research: Planets*, 130(10):e2024JE008889, 2025.

[22] Yan Zhou, Yu-Yan Sara Zhao, Xiaoting Xu, and Yiran Wang. Characteristics and climatic indications of ice-related landforms at low latitudes (0° – $\pm 30^\circ$) on mars. *Remote Sensing*, 17(11):1939, 2025.

[23] Yonggang Xiong, Xueming Xiao, Meibao Yao, Haiqiang Liu, Hong Yang, and Yuegang Fu. Marsformer: Martian rock semantic segmentation with transformer. *IEEE Transactions on Geoscience and Remote Sensing*, 61:1–12, 2023.

[24] Junbo Li, Keyan Chen, Gengju Tian, Lu Li, and Zhenwei Shi. Marsseg: mars surface semantic segmentation with multi-level extractor and connector. *IEEE Transactions on Geoscience and Remote Sensing*, 2025.

[25] Danielle M DeLatte, Sarah T Crites, Nicholas Guttenberg, Elizabeth J Tasker, and Takehisa Yairi. Segmentation convolutional neural networks for automatic crater detection on mars. *IEEE Journal of Selected Topics in Applied Earth Observations and Remote Sensing*, 12(8):2944–2957, 2019.

[26] Jichao Fang, Wei Luo, Qunying Huang, Lei Zhang, Michael Phillips, Venkata Devesh Reddy Seethi, and Iraklis Giannakis. A domain-specific vision foundation model for mars: Self-supervised learning for planetary-scale science discovery. *Authorea Preprints*, 2026.

[27] AM Annex. Mars in focus: Scalable ai unlocks global image search and mapping. *LPI Contributions*, 3090:2064, 2025.

[28] Timothy Paul Nagle-McNaughton, Louis Anthony Scuderi, and Nicholas Erickson. Squeezing data from a rock: Machine learning for martian science. *Geosciences*, 12(6):248, 2022.

[29] Sidiqe Paheding, Abel A Reyes, A Rajaneesh, KS Sajinkumar, and Thomas Oommen. Marsls-net: Martian landslides segmentation network and benchmark dataset. In *Proceedings of the IEEE/CVF Winter Conference on Applications of Computer Vision*, pages 8236–8245, 2024.

[30] Mirali Purohit, Jacob Adler, and Hannah Kerner. Conequest: A benchmark for cone segmentation on mars. In *Proceedings of the IEEE/CVF winter conference on applications of computer vision*, pages 6026–6035, 2024.

[31] Michael Tschannen, Alexey Gritsenko, Xiao Wang, Muhammad Ferjad Naeem, Ibrahim Alabdulmohsin, Nikhil Parthasarathy, Talfan Evans, Lucas Beyer, Ye Xia, Basil Mustafa, et al. Siglip 2: Multilingual vision-language encoders with improved semantic understanding, localization, and dense features. *arXiv preprint arXiv:2502.14786*, 2025.

[32] Daniel Bolya, Po-Yao Huang, Peize Sun, Jang Hyun Cho, Andrea Madotto, Chen Wei, Tengyu Ma, Jiale Zhi, Jathushan Rajasegaran, Hanoona Rasheed, et al. Perception encoder: The best visual embeddings are not at the output of the network. *arXiv preprint arXiv:2504.13181*, 2025.

[33] Haotian Liu, Chunyuan Li, Qingyang Wu, and Yong Jae Lee. Visual instruction tuning. *Advances in neural information processing systems*, 36:34892–34916, 2023.

[34] Shuai Bai, Keqin Chen, Xuejing Liu, Jialin Wang, Wenbin Ge, Sibo Song, Kai Dang, Peng Wang, Shijie Wang, Jun Tang, et al. Qwen2.5-vl technical report. *arXiv preprint arXiv:2502.13923*, 2025.

[35] Zhe Chen, Jiannan Wu, Weihai Wang, Weijie Su, Guo Chen, Sen Xing, Muyan Zhong, Qinglong Zhang, Xizhou Zhu, Lewei Lu, et al. Internvl: Scaling up vision foundation models and aligning for generic visual-linguistic tasks. In *Proceedings of the IEEE/CVF conference on computer vision and pattern recognition*, pages 24185–24198, 2024.

[36] Ting Jiang, Minghui Song, Zihan Zhang, Haizhen Huang, Weiwei Deng, Feng Sun, Qi Zhang, Deqing Wang, and Fuzhen Zhuang. E5-v: Universal embeddings with multimodal large language models. *arXiv preprint arXiv:2407.12580*, 2024.

[37] Xin Zhang, Yanzhao Zhang, Wen Xie, Mingxin Li, Ziqi Dai, Dingkun Long, Pengjun Xie, Meishan Zhang, Wenjie Li, and Min Zhang. Gme: Improving universal multimodal retrieval by multimodal llms. *arXiv preprint arXiv:2412.16855*, 2024.

[38] Rui Meng, Ziyan Jiang, Ye Liu, Mingyi Su, Xinyi Yang, Yuepeng Fu, Can Qin, Zeyuan Chen, Ran Xu, Caiming Xiong, et al. Vlm2vec-v2: Advancing multimodal embedding for videos, images, and visual documents. *arXiv preprint arXiv:2507.04590*, 2025.

[39] Samir Yitzhak Gadre, Gabriel Ilharco, Alex Fang, Jonathan Hayase, Georgios Smyrnis, Thao Nguyen, Ryan Marten, Mitchell Wortsman, Dhruba Ghosh, Jieyu Zhang, et al. Datacomp: In search of the next generation of multimodal datasets. *Advances in Neural Information Processing Systems*, 36:27092–27112, 2023.

[40] Christoph Schuhmann, Romain Beaumont, Richard Vencu, Cade Gordon, Ross Wightman, Mehdi Cherti, Theo Coombes, Aarush Katta, Clayton Mullis, Mitchell Wortsman, et al. Laion-5b: An open large-scale dataset for training next generation image-text models. *Advances in neural information processing systems*, 35:25278–25294, 2022.

[41] Matthijs Douze, Alexandr Guzhva, Chengqi Deng, Jeff Johnson, Gergely Szilvassy, Pierre-Emmanuel Mazaré, Maria Lomeli, Lucas Hosseini, and Hervé Jégou. The faiss library. *IEEE Transactions on Big Data*, 2025.

[42] Yanzhao Zhang, Mingxin Li, Dingkun Long, Xin Zhang, Huan Lin, Baosong Yang, Pengjun Xie, An Yang, Dayiheng Liu, Junyang Lin, et al. Qwen3 embedding: Advancing text embedding and reranking through foundation models. *arXiv preprint arXiv:2506.05176*, 2025.

[43] Alfred S McEwen, Eric M Eliason, James W Bergstrom, Nathan T Bridges, Candice J Hansen, W Alan Delamere, John A Grant, Virginia C Gulick, Kenneth E Herkenhoff, Laszlo Keszthelyi, et al. Mars reconnaissance orbiter’s high resolution imaging science experiment (hirise). *Journal of Geophysical Research: Planets*, 112(E5), 2007.

[44] Alfred S McEwen, Shane Byrne, C Hansen, Ingrid J Daubar, Sarah Sutton, Colin M Dundas, Nicole Bardabelias, Nicole Baugh, J Bergstrom, R Beyer, et al. The high-resolution imaging science experiment (hirise) in the mro extended science phases (2009–2023). *Icarus*, 419:115795, 2024.

[45] Jack Hessel, Ari Holtzman, Maxwell Forbes, Ronan Le Bras, and Yejin Choi. Clipscore: A reference-free evaluation metric for image captioning. In *Proceedings of the 2021 conference on empirical methods in natural language processing*, pages 7514–7528, 2021.

[46] Beier Luo, Shuoyuan Wang, Sharon Li, and Hongxin Wei. Your pre-trained LLM is secretly an unsupervised confidence calibrator. In *The Thirty-ninth Annual Conference on Neural Information Processing Systems*, 2025.

[47] Qwen, :, An Yang, Baosong Yang, Beichen Zhang, Binyuan Hui, Bo Zheng, Bowen Yu, Chengyuan Li, Dayiheng Liu, et al. Qwen2.5 technical report, 2025.

[48] An Yang, Anfeng Li, Baosong Yang, Beichen Zhang, Binyuan Hui, Bo Zheng, and Bowen Yu others. Qwen3 technical report, 2025.

[49] JL Dickson, BL Ehlmann, L Kerber, and CI Fassett. The global context camera (ctx) mosaic of mars: A product of information-preserving image data processing. *Earth and space Science*, 11(7):e2024EA003555, 2024.

[50] A. M. Morgan, S. A. Wilson, and A. D. Howard. The global distribution and morphologic characteristics of fan-shaped sedimentary landforms on Mars. *Icarus*, 385:115137, 2022.

[51] C. Souness, B. Hubbard, R. E. Milliken, and D. Quincey. An inventory and population-scale analysis of martian glacier-like forms. *Icarus*, 217:243–255, 2012.

[52] K. P. Roback and B. L. Ehlmann. Controls on the global distribution of martian landslides. *J. Geophys. Res. Planets*, 126:e2020JE006675, 2021.

[53] M. M. Mills, V. T. Bickel, A. S. McEwen, and A. Valantinas. A global dataset of pitted cones on Mars. *Icarus*, 418:116145, 2024.

[54] J. Liu et al. Mapping and spatial statistical analysis of Mars Yardangs. *Planet. Space Sci.*, 192:105035, 2020.

[55] Jon Louis Bentley. Multidimensional binary search trees used for associative searching. *Communications of the ACM*, 18(9):509–517, 1975.

[56] Alex Fang, Albin Madappally Jose, Amit Jain, Ludwig Schmidt, Alexander Toshev, and Vaishaal Shankar. Data filtering networks. *arXiv preprint arXiv:2309.17425*, 2023.

[57] Junjie Zhou, Yongping Xiong, Zheng Liu, Ze Liu, Shitao Xiao, Yueze Wang, Bo Zhao, Chen Jason Zhang, and Defu Lian. Megapairs: Massive data synthesis for universal multimodal retrieval. In *Proceedings of the 63rd Annual Meeting of the Association for Computational Linguistics (Volume 1: Long Papers)*, pages 19076–19095, 2025.

[58] Enrico Fini, Mustafa Shukor, Xiujun Li, Philipp Dufter, Michal Klein, David Haldimann, Sai Aitharaju, Victor G Turrisi da Costa, Louis Béthune, Zhe Gan, et al. Multimodal autoregressive pre-training of large vision encoders. In *Proceedings of the Computer Vision and Pattern Recognition Conference*, pages 9641–9654, 2025.

[59] Xiaohua Zhai, Basil Mustafa, Alexander Kolesnikov, and Lucas Beyer. Sigmoid loss for language image pre-training. In *Proceedings of the IEEE/CVF international conference on computer vision*, pages 11975–11986, 2023.

[60] Raghuvir Thirukovalluru, Rui Meng, Ye Liu, Mingyi Su, Ping Nie, Semih Yavuz, Yingbo Zhou, Wenhui Chen, Bhuvan Dhingra, et al. Breaking the batch barrier (b3) of contrastive learning via smart batch mining. *arXiv preprint arXiv:2505.11293*, 2025.

[61] Michael Günther, Saba Sturua, Mohammad Kalim Akram, Isabelle Mohr, Andrei Ungureanu, Bo Wang, Sedigheh Eslami, Scott Martens, Maximilian Werk, Nan Wang, et al. jina-embeddings-v4: Universal embeddings for multimodal multilingual retrieval. In *Proceedings of the 5th Workshop on Multilingual Representation Learning (MRL 2025)*, pages 531–550, 2025.

[62] OpenSearch AI. Opensearch-ai/ops-mm-embedding-v1-2b. <https://huggingface.co/OpenSearch-AI/Ops-MM-embedding-v1-2B>, 2025.

A Dataset Construction

A.1 Paired Image–Text Retrieval

Confidence Estimation. For both the LLM-based domain relevance filtering and the VLM-based consistency filtering, the confidence score is derived from the model’s output logits during a single-token inference step. we use a confidence score that represents the likelihood of a caption being related to Mars. Specifically, we extract the raw logits corresponding to the target tokens “yes” and “no”. To obtain a confidence value, we apply a softmax function over these two logits to compute the normalized probability of the “yes” token:

$$\text{Confidence} = \frac{\exp(L_{\text{yes}})}{\exp(L_{\text{yes}}) + \exp(L_{\text{no}})},$$

where L_{yes} and L_{no} represent the logit values for the respective tokens. This probability value serves as the final confidence score [46]. The prompt template for LLM and MLLM confidence are shown in Figure 8 and Figure 9.

Data Filtering. As we mentioned in Section 4.1, we implemented a data filtering strategy based on three metrics to ensure the relevance and quality of the image-text pairs in our dataset construction of task 1. Specifically, we apply multi-modal filtering using the following thresholds: the CLIP score for text-image semantic alignment with a threshold of $\tau_{\text{clip}} = 0.32$, the LLM relevance confidence for Mars-specific grounding with a threshold of $\tau_{\text{llm}} = 0.82$, and the MLLM consistency score for visual support of the claimed Martian features with a threshold of $\tau_{\text{mllm}} = 0.82$. A candidate pair is retained only when all three scores exceed the respective thresholds.

A.2 Landform Retrieval

Prompt Ensemble. In Landform Retrieval (Task 2), we employ a prompt ensembling strategy to generate a robust prototype query embedding for each geomorphic subclass by averaging the output embeddings from the model’s text encoder across multiple linguistic variations. To rigorously evaluate the sensitivity of our retrieval-centric protocol to these variations, we conducted an ablation study using ten distinct candidate templates, as detailed in Table 5. These templates are designed to capture diverse scientific and observational perspectives, specifically: “a photo of , a type of martian terrain”, “a satellite photo of ”, “a high-resolution remote sensing image of on Mars”, “a detailed satellite view of geomorphic feature from Mars”, “an aerial perspective of morphological structure on Mars”, “high-definition remote sensing photo of on the red planet”, “a CTX or HiRISE image showing terrain on Mars”, “an orbital image of landform on the Martian surface”, “Martian as captured in space-based imagery”, and “planetary-scale capture of in Martian geology”. Our experiments demonstrate that while increasing the number of templates can yield performance gains for domain-specialized models like MarScope, the incremental benefit for most general foundation models tends to saturate at three templates. Based on these findings, we adopted an ensemble of the first 3 templates as the default setting throughout the paper.

A.3 Global Geo-Localization

Image-based Retrieval. To provide a comprehensive evaluation of model performance in Global Geo-Localization, we utilize both text-based and image-based queries to estimate the planetary-scale distribution of Martian landforms. For each target landform category, we select a small set of query images (Alluvial Fans: 8, Glacier-Like Form: 8, Landslides: 10, Pitted cones: 8, Yardangs: 18), which is manually curated by planetary scientists. For visualization, we show 6 random query examples per class in Figure 11.

Prompt template for LLM-based filtering in Paired Image–Text Retrieval (Task 1)

You are a planetary science expert data classifier.

Evaluate the following image descriptions.

Determine if the image is related to Mars (the planet) or Martian context (surface, rovers, orbiters, geology).

Input Data:

$\langle \text{image_caption} \rangle$

Task:

- Answer “Yes” if the descriptions are related to Mars or Martian planetary science.
- Answer “No” if they are NOT related to Mars or if the information is uncertain or ambiguous.

Return ONLY one word: “Yes” or “No”.

Prompt template for MLLM-based filtering in Paired Image–Text Retrieval (Task 1)

Instruction

You are an expert planetary science data classifier. Your task is to analyze the image and caption to determine if they are specifically related to Mars (the planet) or Martian context (surface, rovers, orbiters, geology).

Definitions

YES (Mars or Martian Science):

- **Subjects:** Mars (the planet), Martian surface, Mars rovers (e.g., Perseverance), Mars orbiters, Martian geology.
- **Surface Features:** Images related to Mars’ surface features, such as craters, regolith, dunes, volcanoes, and valleys on Mars.
- **Spacecraft:** Photos or data from Mars spacecraft (rovers, orbiters, landers) and scientific data from Mars missions.
- **Scientific Data:** Spectra, geological maps, and any data related to Mars or its satellites.

NO (Not Mars or Martian Science):

- **Earth Context:** Any Earth-related content, such as Earth landscapes, cities, or forests.
- **Astronomy or Astrophysics:** Deep space images, nebulae, galaxies, or objects unrelated to Mars.
- **Artificial/Fake:** Sci-fi, CGI renders, video game screenshots, or concept art.
- **Irrelevant:** Humans, selfies, museum exhibits, and Earth-based telescope equipment.

Constraint

- Focus strictly on Mars or Martian content. Exclude anything that is not directly related to Mars or its context.
- If the image looks like a video game or art, answer “no” even if the caption mentions Mars.

Input Data

Image: $\langle \text{input_image} \rangle$

Caption: “ $\langle \text{image_caption} \rangle$ ”

Return ONLY one word: “Yes” or “No”.

B Evaluation Metrics

B.1 Paired Image–Text Retrieval

To systematically evaluate the cross-modal alignment capabilities of Vision-Language Models (VLMs) in the planetary science domain, we formulate Task 1 as a bidirectional retrieval problem. Given a set of N paired Martian image–text instances $\mathcal{D} = \{(i_k, t_k)\}_{k=1}^N$, for each query in one modality (e.g., a text description t_j), the model is required to rank all N candidates in the opposite modality (e.g., images $\{i_1, \dots, i_N\}$) based on their cosine similarity. The retrieval performance is evaluated on several widely-used metrics that capture both the accuracy and quality of ranking:

Prompt template for MLLM-based caption refinement in Paired Image–Text Retrieval (Task 1)

You are a planetary science captioner for multimodal datasets.

Input Data

IMAGE: $\langle \text{input_image} \rangle$

CAPTION: “ $\langle \text{image_caption} \rangle$ ”

Task:

Analyze the IMAGE and CAPTION to write ONE caption draft.

Hard Rules:

1) Visual Grounding (PRIORITY):

- Describe visible attributes (shape, texture, brightness, etc.) derived from the IMAGE.
- **Exception for Composition:** You MAY use composition terms ONLY if they are explicitly present in the caption and match the visual appearance.

2) Entity-First Structure:

- Start with the primary target / feature name from CAPTION.
- **BANNED:** Do not start with “The image shows”, “A view of”, etc.

3) Anchor Logic:

- Use CAPTION for **Identity** (Subject Name, Location, Instrument).
- Describe IMAGE with precise planetary geology terms.
- If CAPTION describes features NOT visible in the crop, IGNORE them.

4) Noise Removal:

- Ignore IDs, coordinates, timestamps, and narrative fluff.

Style:

- Scientific, neutral, information-dense.

Return STRICT JSON only:

{ “refined_caption”: “ $\langle \text{your_caption} \rangle$ ” }

Recall@K (R@K) This metric measures the proportion of queries for which the ground-truth match appears within the top-K ranked candidates, which can be formally defined as:

$$R@K = \frac{1}{N} \sum_{j=1}^N \mathbb{I}(r_j \leq K),$$

where $\mathbb{I}(\cdot)$ is the indicator function. We report **R@1** and **R@10** to assess high-precision and top-tier retrieval performance.

MRR Mean Reciprocal Rank (MRR) rewards the models for ranking the correct match as high as possible and is defined as:

$$MRR = \frac{1}{N} \sum_{j=1}^N \frac{1}{r_j}.$$

MedR To evaluate the overall stability of the model’s representation space and mitigate the influence of extreme outliers, we report the Median Rank (MedR):

$$\text{MedR} = \text{median}(\{r_1, r_2, \dots, r_N\}).$$

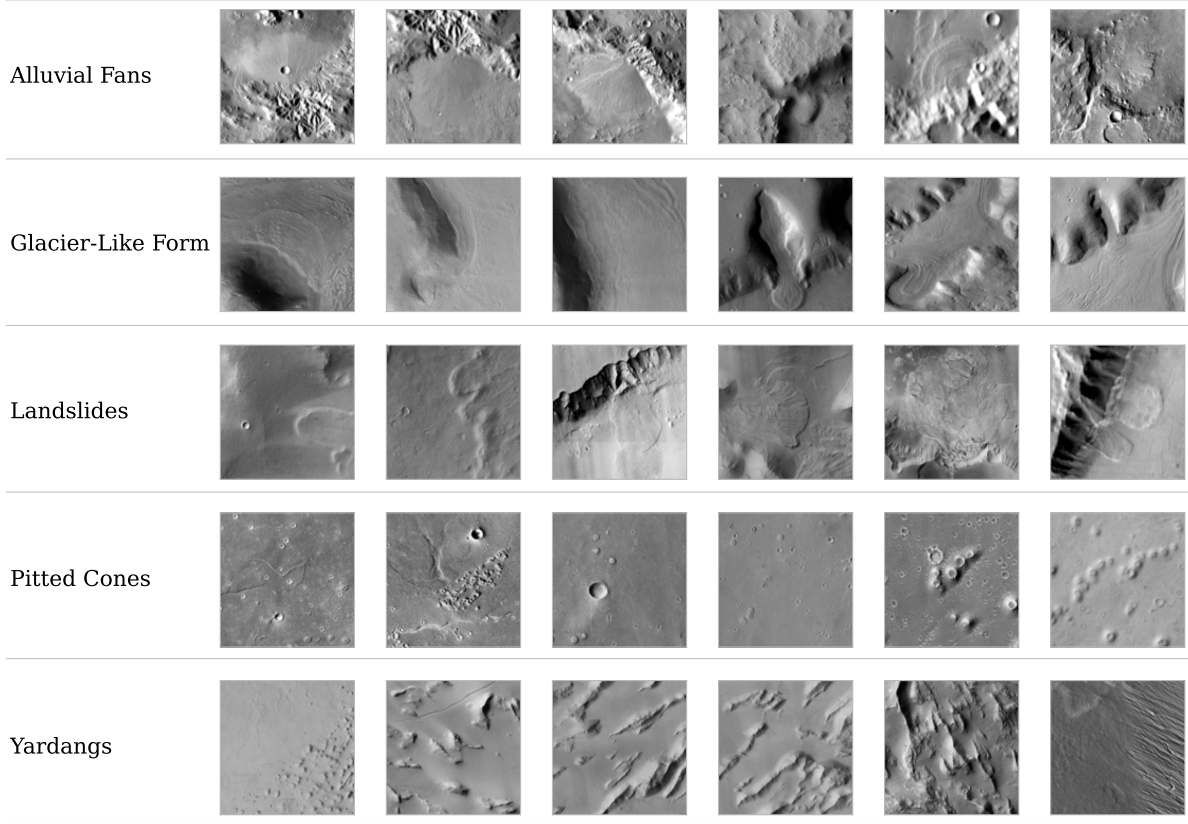


Figure 11: Image-based query examples for Task 3 (Global Geo-Localization)

A lower MedR indicates a more robust and consistent alignment across the entire paired vision-language retrieval dataset.

B.2 Landform Retrieval

We evaluate the task of landform retrieval in a text-to-image multi-positive setting, where each query is encoded from a Martian landform and needs to retrieve multiple relevant images. Let $\{x_1, x_2, \dots, x_N\}$ be the ranked list of database images for query q , and $\text{rel}_i \in \{0, 1\}$ be the binary relevance indicator where $\text{rel}_i = 1$ if $x_i \in \mathcal{G}_q$. We employ the following metrics to conduct evaluation under the long-tailed distribution of the 48 categories:

mAP (macro) We evaluate retrieval performance using mean Average Precision (mAP) computed as a uniform (macro) average over C text queries $\{q_c\}_{c=1}^C$ (one per landform category). For a query q_c , given the ranked list of database images $\{x_i\}_{i=1}^N$ and relevance indicators $\text{rel}_i = \mathbb{1}[x_i \in \mathcal{G}_{q_c}]$, the Average Precision (AP) is:

$$\text{AP}(q_c) = \frac{1}{|\mathcal{G}_{q_c}|} \sum_{i=1}^N P@i \cdot \text{rel}_i, \quad P@i = \frac{\sum_{j=1}^i \text{rel}_j}{i}.$$

$$\text{mAP} = \frac{1}{C} \sum_{c=1}^C \text{AP}(q_c).$$

nDCG@10 To evaluate whether the most representative instances are prioritized in the top-tier results, we report the Normalized Discounted Cumulative Gain at cutoff 10. For the query q_c associated with category c :

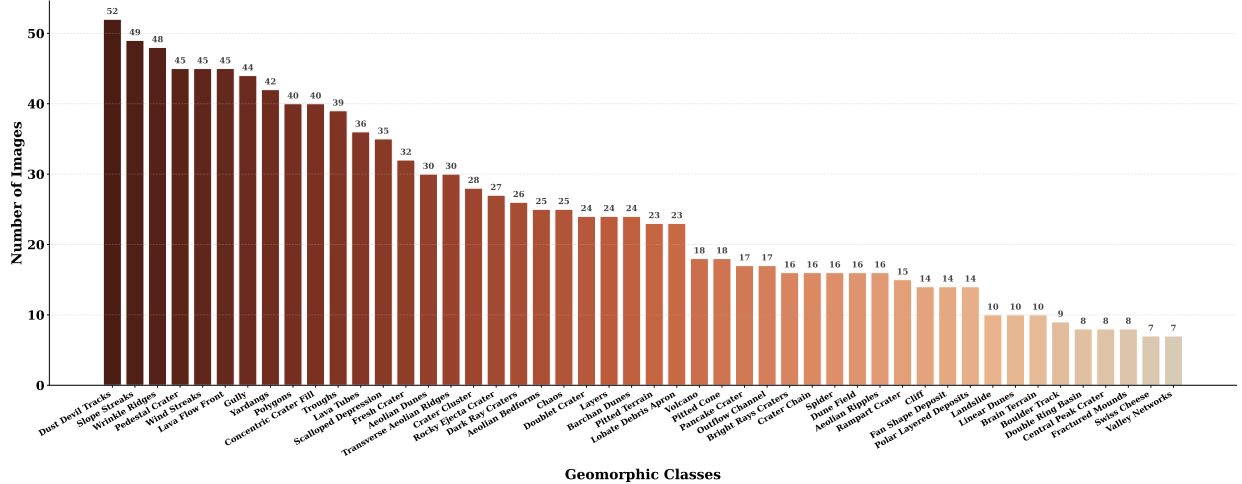


Figure 12: Sample distribution of the 48 long-tailed geomorphic categories utilized in Landform Retrieval (Task 2).

$$\text{DCG@10}(q_c) = \sum_{i=1}^{10} \frac{\text{rel}_i}{\log_2(i+1)}, \quad \text{nDCG@10} = \frac{1}{C} \sum_{c=1}^C \frac{\text{DCG@10}(q_c)}{\text{IDCG@10}(q_c)},$$

where $IDCG@10(q_c)$ is the ideal DCG obtained by ranking all available positives for q_c at the top of the list (up to the cutoff 10) and applying the same DCG@10 definition.

Hits@10 This measures the model's ability to find at least one correct instance within the top 10 results:

$$\text{Hits}@10 = \frac{1}{C} \sum_{q=1}^C \mathbb{I} \left(\sum_{i=1}^{10} \text{rel}_i > 0 \right).$$

B.3 Global Geo-Localization

In Task 3, we evaluate a model's ability to estimate the planetary-scale spatial distribution of Martian landforms. Given the extreme sparsity of positive samples within the global CTX mosaic (~ 1.4 million tiles), we formulate this as a proximity-based point-set matching problem in a projected coordinate space.

To ensure computational efficiency across the global dataset, we map all geographic coordinates (lon, lat) onto a global equirectangular (Plate Carrée) mosaic with a fixed resolution. A retrieved image patch is considered a true positive if its projected center coordinate \mathbf{p}' falls within a pixel-wise Euclidean distance r_{px} of a projected ground-truth entry \mathbf{g}' :

$$\|\mathbf{p}' - \mathbf{g}'\|_2 \leq r_{px}.$$

The pixel-wise tolerance r_{px} is derived from a spatial angular radius r (set to 0.5°) as: $r_{px} = r \cdot (W/360^\circ)$.

For a retrieval depth K , let $\mathcal{P}'_K = \{\mathbf{p}'_1, \mathbf{p}'_2, \dots, \mathbf{p}'_K\}$ be the projected coordinates of the top- K retrieved tiles, and $\mathcal{G}' = \{\mathbf{g}'_1, \mathbf{g}'_2, \dots, \mathbf{g}'_M\}$ be the M projected reference points from the catalogue. We define the foundational metrics as follows:

Precision(K) This metric measures retrieval fidelity, representing the fraction of predicted tiles spatially validated by the catalogue in the projected space:

$$\text{Precision}(K) = \frac{1}{K} \sum_{i=1}^K \mathbb{I} \left(\min_{\mathbf{g}' \in \mathcal{G}'} \|\mathbf{p}'_i - \mathbf{g}'\|_2 \leq r_{px} \right).$$

Recall(K) This metric measures mapping completeness, representing the fraction of catalogue entries successfully recovered within the tolerance radius:

$$\text{Recall}(K) = \frac{1}{M} \sum_{j=1}^M \mathbb{I} \left(\min_{\mathbf{p}' \in \mathcal{P}_K} \|\mathbf{p}' - \mathbf{g}'_j\|_2 \leq r_{px} \right).$$

Based on the Precision and Recall defined above, we report the following cumulative metrics to characterize the global localization performance:

Area Under Precision-Recall Curve (AUPRC) AUPRC assesses the trade-off between retrieval precision and recall across all sensitivity levels (retrieval depths). We define it as:

$$\text{AUPRC} = \int_0^1 \text{Precision}(\rho) d\rho, \quad \rho = \text{Recall}.$$

In practice, the PR curve is obtained by sweeping the retrieval depth K , and the integral is approximated using trapezoidal integration over the sampled points $\{(\text{Recall}(K), \text{Precision}(K))\}_K$.

F1@ K^* To quantify the optimal balance between mapping fidelity and completeness, we report the maximum F1-score achievable on the PR curve. The F1-score at depth K is defined as:

$$\text{F1}(K) = 2 \cdot \frac{\text{Precision}(K) \cdot \text{Recall}(K)}{\text{Precision}(K) + \text{Recall}(K)}.$$

We specifically report the peak performance $\text{F1}@K^* = \max_K \text{F1}(K)$, where K^* represents the optimal retrieval depth for the specific model.

C Experimental Results

C.1 Paired Image–Text Retrieval

Raw captions substantially degrade paired image–text alignment. To further evaluate the impact of data quality on vision-language alignment, we report the performance of Task 1 with their raw caption in Table 7. Compared to the results with refined captions in Table 2, all evaluated models exhibit a significant performance degradation when utilizing raw data. This decline suggests that raw Martian descriptions from web-scale corpora often contain substantial noise (e.g., internal IDs, coordinates, or narrative fluff), which interferes with the cross-modal feature alignment. These findings reinforce the conclusion that high-quality caption refinement is a critical prerequisite for effective planetary science discovery.

C.2 Landform Retrieval

The performance of MarScope attributes to generalization rather than memorization. To address potential selection bias arising from MarScope for the initial data collection in Task 2, we further evaluate models on a subset of landform classes that were constructed without using MarScope, including *Boulder Track*, *Brain Terrain*, *Double Ring Basin*, *Fractured Mounds*, *Rocky Ejecta Crater*, *Swiss Cheese*, and *Valley Networks*. These images are specifically curated via manual expert search from high-resolution CTX and HiRISE imagery. As shown in Table 8, the results remain consistent that MarScope still achieves a dominant performance than general foundation models like PE-Core and Qwen3-VL-Embedding. These results demonstrate that the effectiveness of domain-specific models stems from geomorphic generalization rather than a "memorization" of discovery-based patterns, thereby confirming the fairness of the MarsRetrieval evaluation.

C.3 Global Geo-Localization

Optimal F1 further emphasizes the importance of domain-specific post-training. Table 9 provides a detailed comparison of the optimal F1-score ($F1@K^*$) across various models for Task 3 (Global Geo-Localization). The results highlight the dominance of the domain-specialized model MarScope, which significantly outperforms general foundation models. This gap underscores that general multimodal representations lack the specialized planetary knowledge required to establish precise links between scientific terminology and subtle geomorphic structures. In summary, without explicit planetary-domain fine-tuning, generic representations are insufficient for precise planetary-scale discovery.

Table 7: Performance comparison of different models on Paired Image–Text Retrieval (Task 1) with raw (unrefined) captions. Notably, performance across all models is significantly lower compared to the results with refined captions (see Table 2). Bold indicates the best result, while underlining denotes the second-best.

| Model | Backbone | Size | T→I | | | | I→T | | | |
|-----------------------------|------------|------|--------------|--------------|--------------|-----------|--------------|--------------|--------------|-----------|
| | | | R@1 | R@10 | MRR | MedR | R@1 | R@10 | MRR | MedR |
| <i>Encoder-based Models</i> | | | | | | | | | | |
| DFN2B-CLIP-ViT-L-14 | ViT-L/14 | 0.4B | 8.05 | 20.73 | 12.58 | 130 | 8.26 | 22.47 | 12.92 | 116 |
| ViT-L-16-SigLIP-384 | ViT-L/16 | 0.4B | 9.01 | 20.24 | 13.02 | 176 | 11.28 | 22.43 | 15.27 | 167 |
| BGE-VL-large | ViT-L/14 | 0.4B | 1.31 | 4.11 | 2.59 | 551 | 4.15 | 11.72 | 6.86 | 298 |
| aimv2-large-patch14-224 | ViT-L/14 | 0.4B | 4.77 | 14.12 | 8.09 | 241 | 4.68 | 14.43 | 8.11 | 233 |
| ViT-L-16-SigLIP2-512 | ViT-L/16 | 0.4B | 12.42 | 26.98 | 17.34 | 87 | 13.16 | 27.72 | 18.21 | 89 |
| PE-Core-L-14-336 | ViT-L/14 | 0.4B | 16.44 | 37.04 | 23.57 | 27 | 17.01 | 38.35 | 24.42 | 24 |
| MarScope (DFN2B) | ViT-L/14 | 0.4B | <u>14.25</u> | <u>34.67</u> | <u>21.15</u> | <u>39</u> | <u>13.73</u> | <u>37.69</u> | <u>21.77</u> | <u>29</u> |
| <i>MLLM-based Models</i> | | | | | | | | | | |
| E5-V | LLaVA-Next | 8B | 5.90 | 12.11 | 8.25 | 451 | 8.92 | 15.78 | 11.57 | 350 |
| gme | Qwen2-VL | 2B | 7.52 | 16.40 | 10.76 | 286 | 9.44 | 19.59 | 13.07 | 220 |
| B3++ | Qwen2-VL | 2B | 0.96 | 4.98 | 2.54 | 615 | 3.19 | 9.40 | 5.60 | 442 |
| jina-embeddings-v4 | Qwen2.5-VL | 3B | 5.95 | 13.12 | 8.65 | 377 | 8.61 | 15.52 | 11.36 | 336 |
| VLM2Vec-V2.0 | Qwen2-VL | 2B | 1.22 | 4.85 | 2.71 | 546 | 4.20 | 10.80 | 6.59 | 396 |
| Ops-MM-embedding-v1 | Qwen2-VL | 2B | 9.14 | 18.23 | 12.33 | 287 | 11.98 | 21.86 | 15.77 | 180 |
| Qwen3-VL-Embedding | Qwen3-VL | 2B | 6.03 | 14.08 | 8.82 | 372 | 9.75 | 18.10 | 12.87 | 272 |

Table 8: Dataset bias analysis on Task 2. We report the results on landform classes constructed without using MarScope.

| Model | mAP | nDCG@10 | Hits@10 |
|--------------------|--------------|--------------|--------------|
| PE-Core-L-14-336 | 14.74 | 17.54 | 71.43 |
| Qwen3-VL-Embedding | 2.75 | 10.05 | 39.58 |
| MarScope | 52.35 | 54.71 | 85.71 |

Text queries produce distributions more consistent with global catalogues. To qualitatively assess retrieval effectiveness, we visualize the global geomorphic distributions generated by MarScope in Figure 14. By comparing the predicted maps against the human-curated ground truth catalogs, it is evident that MarScope’s predicted global distributions against catalogue-based ground truth. For categories such as Pitted Cones and Glacier-like forms, text queries accurately capture the latitudinal distribution of these landforms. While image-based retrieval successfully identifies major clusters, it is more prone to false positives from geomorphically similar but unrelated terrains. These results support the potential of language-driven retrieval for scalable planetary mapping.

Text-based retrieval shows stronger peak performance and better stability. Figure 13 illustrates the sensitivity of the F1-score to the retrieval depth K in Task 3. The results shows that text queries typically achieve higher peaks and e and superior stability across different values of K . This reflects the inherent intra-class visual diversity of Martian landforms, where a limited set of image exemplars cannot fully represent the morphological evolution of a category across the entire planet.

Table 9: Performance comparison of Global Geo-Localization (Task 3) measured by the optimal F1-score ($F1@K^*$). The domain-specialized MarScope significantly outperforms all general foundation models. This gap highlights the necessity of explicit fine-tuning with planetary knowledge for precise large-scale scientific discovery. Bold indicates the best result, while underlining denotes the second-best.

| Model | Alluvial Fans | | Glacier-Like Forms | | Landslides | | Pitted Cones | | Yardangs | |
|-----------------------------|---------------|--------------|--------------------|--------------|--------------|--------------|--------------|--------------|--------------|--------------|
| | Text | Image | Text | Image | Text | Image | Text | Image | Text | Image |
| <i>Encoder-based Models</i> | | | | | | | | | | |
| DFN2B-CLIP-ViT-L-14 | 6.19 | 7.94 | 7.16 | 34.98 | 47.90 | 13.69 | 19.38 | 36.52 | 2.92 | 47.11 |
| ViT-L-16-SigLIP-384 | <u>16.26</u> | 6.71 | 7.69 | 24.89 | 38.73 | 8.95 | 17.12 | 29.13 | 7.97 | 51.75 |
| BGE-VL-large | 6.44 | 8.89 | 7.19 | 22.99 | <u>48.47</u> | 17.44 | 10.16 | <u>41.54</u> | 7.92 | 33.68 |
| aimv2-large-patch14-224 | 6.83 | 4.67 | 8.02 | 24.76 | 42.63 | 8.84 | 9.51 | 28.80 | 6.41 | 38.01 |
| ViT-L-16-SigLIP2-512 | 7.13 | 9.38 | <u>15.32</u> | 39.40 | 42.96 | 9.82 | 15.47 | 32.32 | 8.01 | 46.21 |
| PE-Core-L-14-336 | 13.82 | 7.47 | 15.02 | 29.54 | 48.82 | 16.36 | <u>34.69</u> | 36.93 | 8.94 | 51.47 |
| MarScope | 31.93 | 26.51 | 52.57 | 55.58 | 42.44 | 27.40 | 83.24 | 56.02 | 80.39 | 73.98 |
| <i>Vision-only Models</i> | | | | | | | | | | |
| aimv2-large-patch14-448 | – | 7.42 | – | 33.96 | – | <u>18.86</u> | – | 33.28 | – | 35.04 |
| dinov3-vitl16 | – | <u>12.27</u> | – | <u>43.06</u> | – | 12.33 | – | 32.50 | – | <u>62.95</u> |
| <i>MLLM-based Models</i> | | | | | | | | | | |
| E5-V | 11.37 | 10.37 | 7.85 | 22.98 | 40.23 | 11.42 | 6.44 | 35.91 | 8.57 | 39.54 |
| gme | 4.71 | <u>5.75</u> | <u>6.79</u> | 29.74 | 12.11 | 10.49 | 3.82 | 23.27 | 2.72 | 44.83 |
| B3++ | 0.68 | <u>5.39</u> | 2.77 | 18.23 | 0.89 | 11.51 | 1.48 | 30.56 | 0.18 | 54.67 |
| jina-embeddings-v4 | 7.34 | 2.22 | <u>5.87</u> | 15.32 | 8.80 | 6.00 | 4.98 | 39.99 | 5.45 | 27.73 |
| VLM2Vec-V2.0 | 5.68 | <u>6.51</u> | 2.65 | 9.21 | 9.13 | 16.10 | 9.70 | 20.88 | 2.58 | 54.21 |
| Ops-MM-embedding-v1 | 9.26 | <u>5.15</u> | 8.49 | 25.26 | 22.56 | 9.34 | 13.76 | 36.55 | 3.77 | 55.12 |
| Qwen3-VL-Embedding | 5.84 | 3.29 | 3.77 | 26.41 | 17.52 | 8.83 | 3.00 | 18.13 | <u>21.40</u> | 57.49 |

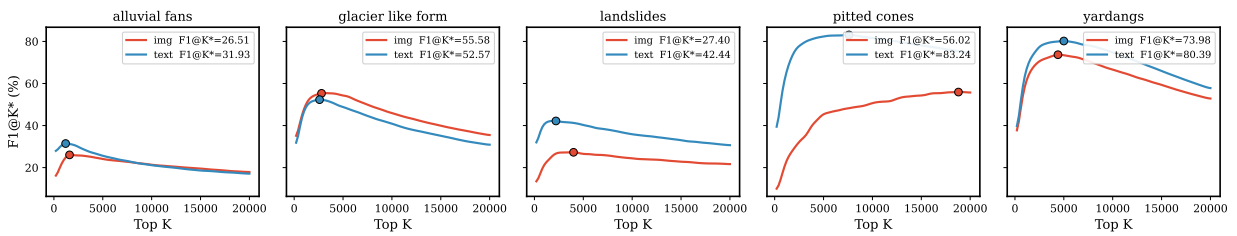


Figure 13: Sensitivity of ($F1@K$) to retrieval depth K in task 3. Text-based queries exhibit better peak performance and stability.

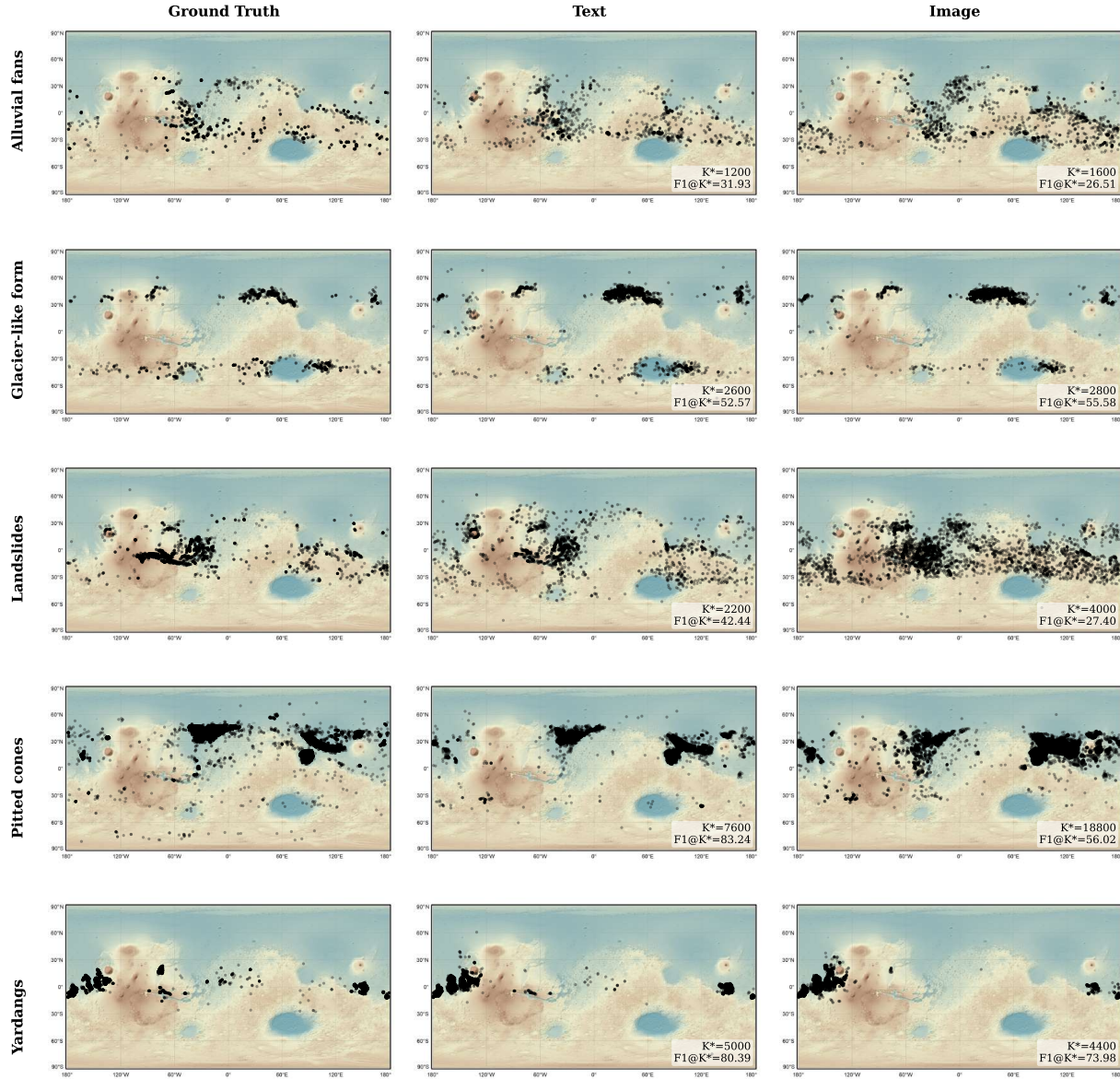


Figure 14: The visualization of planetary-scale geomorphic distributions generated by MarScope (Task 3). MarScope's text-based retrieval produces distributions that are more consistent with global catalogues compared to image-based retrieval.